Inorganic Chemistry
Article
pubs.acs.org/IC

Cation Ordering and Flexibility of the BO_4^{2-} Tetrahedra in Incommensurately Modulated $CaEu_2(BO_4)_4$ (B = Mo, W) Scheelites

Artem M. Abakumov,*[†] Vladimir A. Morozov,[†,‡] Alexander A. Tsirlin,[§] Johan Verbeeck,[†] and Joke Hadermann[†]

[†]EMAT, University of Antwerp, Groenenborgerlaan 171, B-2020 Antwerp, Belgium
[‡]Chemistry Department, Moscow State University, 119991 Moscow, Russia
[§]National Institute of Chemical Physics and Biophysics, 12618 Tallinn, Estonia

Supporting Information

ABSTRACT: The factors mediating cation ordering in the scheelite-based molybdates and tungstates are discussed on the basis of the incommensurately modulated crystal structures of the $CaEu_2(BO_4)_4$ (B = Mo, W) red phosphors solved from high-resolution synchrotron powder X-ray diffraction data. Monoclinic $CaEu_2(WO_4)_4$ adopts a (3 + 1)-dimensionally modulated structure [superspace group $I2/b(\alpha\beta0)00$, $a = 5.238\,73(1)$ Å, $b = 5.266\,35(1)$ Å, $c = 11.463\,19(9)$ Å, $\gamma = 91.1511(2)°$, $\mathbf{q} = 0.56153(6)\mathbf{a}^* + 0.7708(9)\mathbf{b}^*$, $R_F = 0.050$, $R_P = 0.069$], whereas tetragonal $CaEu_2(MoO_4)_4$ is (3 + 2)-dimensionally modulated [superspace group $I4_1/a(\alpha\beta0)00(-\beta\alpha0)00$, $a = 5.238\,672(7)$ Å, $c = 11.548\,43(2)$ Å, $\mathbf{q}_1 = 0.55331(8)\mathbf{a}^* + 0.82068(9)\mathbf{b}^*$, $\mathbf{q}_2 = -0.82068(9)\mathbf{a}^* + 0.55331(8)\mathbf{b}^*$, $R_F = 0.061$, $R_P = 0.082$]. In both cases the modulation arises from the ordering of the Ca/Eu cations and the cation vacancies at the A-sublattice of the parent scheelite ABO_4 structure. The cation ordering is incomplete and better described with harmonic rather than with steplike occupational modulation functions. The structures respond to the variation of the effective charge and cation size at the A-position through the flexible geometry of the MoO_4^{2-} and WO_4^{2-} tetrahedra demonstrating an alternation of stretching the B−O bond lengths and bending the O−B−O bond angles. The tendency towards A-site cation ordering in scheelites is rationalized using the difference in ionic radii and concentration of the A-site vacancies as parameters and presented in the form of a structure map.

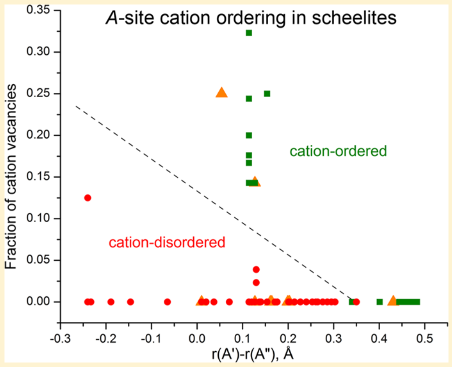

1. INTRODUCTION

Scheelite ($CaWO_4$) related compounds $(A',A'')_n(BO_4)_m$ with B = W and/or Mo are promising materials for phosphors in pc-WLEDs (phosphor-converted white-light-emitting-diode) and solid-state lasers.[1−6] Scheelites can be prepared with a large concentration of vacancies in the A sublattice, yielding compositions characterized by an A:B ratio different from 1:1. The creation of cation vacancies in the scheelite-type framework and the ordering of the A-cations and vacancies are a new factor in controlling the scheelite-type structure and properties.[7,8] Very often the population of the A-sites in the scheelite-type structure by cations with different sizes and charges (such as alkali metal cations M^+ and rare-earth cations R^{3+}) and/or cation vacancies leads to modulated structures with a pronounced occupational modulation wave.[7,9−12]

Recently, we have studied the luminescent properties of the $CaGd_{2(1-x)}Eu_{2x}(MoO_4)_{4(1-y)}(WO_4)_{4y}$ ($0 \le x \le 1$, $0 \le y \le 1$) solid solutions with the scheelite-type structure.[13] These phosphors emit intense red light dominated by the $^5D_0$−$^7F_2$ transition at 612 nm. Moreover, the temperature dependence of the ratio of the $^5D_1$ to $^5D_0$ emission intensity enables these materials to visualize temperature gradients with high accuracy and spatial resolution, making them excellent thermographic phosphors.[14] In that recent study, only a rough structure model has been constructed for (3 + 1)-dimensional [(3+1)D] incommensurately modulated monoclinic $CaEu_2(WO_4)_4$ using precession electron diffraction (PED) data. We demonstrated that the replacement of the smaller Gd^{3+} by the larger Eu^{3+} at the A sublattice does not affect the nature of the incommensurate modulation, but an increasing replacement of W^{6+} by Mo^{6+} switches the modulation from the (3+1)D to the (3+2)D regime. In this contribution, we provide the structure solution for (3+1)D-modulated monoclinic $CaEu_2(WO_4)_4$ and (3+2)D-modulated tetragonal $CaEu_2(MoO_4)_4$ using high-resolution synchrotron powder X-ray diffraction and discuss the behavior and role of the MoO_4^{2-} and WO_4^{2-} tetrahedral units in the A-site cation ordering.

2. EXPERIMENTAL SECTION

The synthesis and preliminary characterization of the $CaEu_2(BO_4)_4$ (B = Mo, W) samples have been described elsewhere.[13] High-resolution synchrotron X-ray powder diffraction (SXPD) data were collected at room temperature at the ID31 beamline of the European Synchrotron Radiation Facility (ESRF, Grenoble, France) using a constant wavelength of $\lambda \approx 0.4$ Å and eight scintillation detectors, each preceded by a Si(111) analyzer crystal. The powder samples were placed in a thin-walled borosilicate glass capillary that was spun during the experiment.

Received: June 29, 2014
Published: August 21, 2014

dx.doi.org/10.1021/ic5015412 | *Inorg. Chem.* 2014, 53, 9407−9415

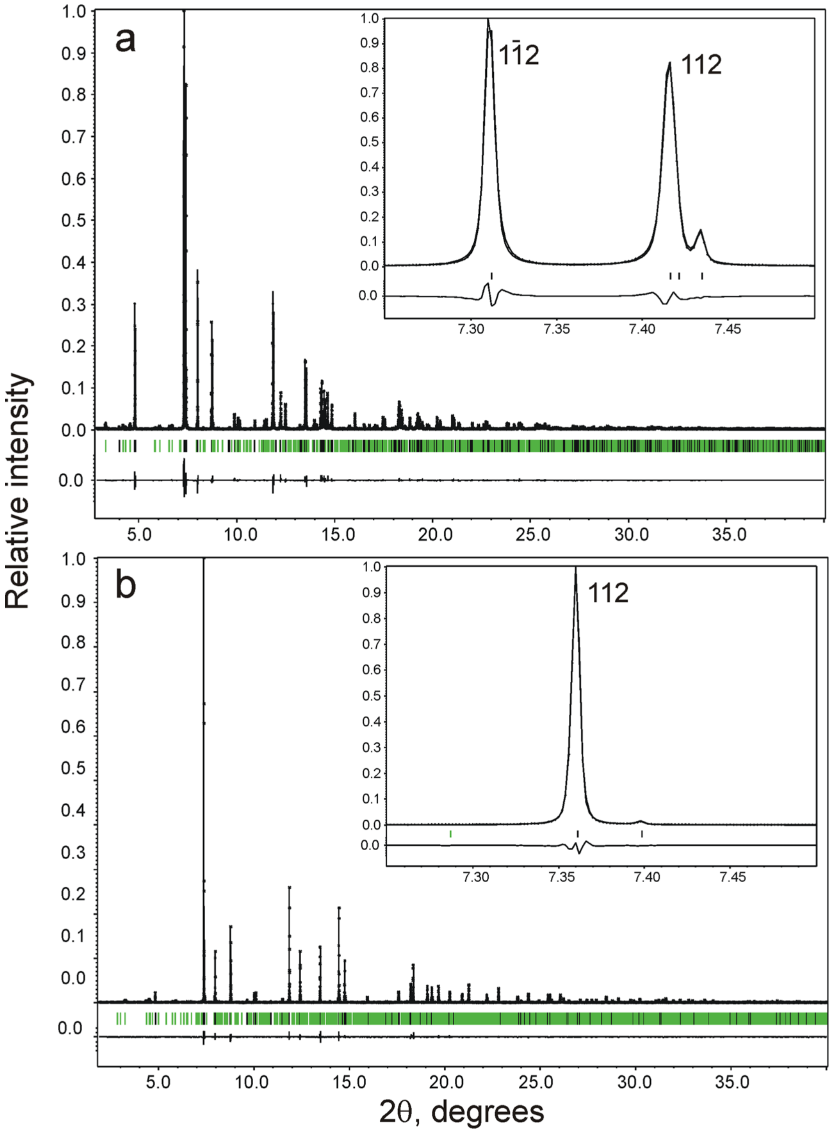

Figure 1. Experimental, calculated, and difference SXPD profiles after Rietveld refinement of the $CaEu_2(WO_4)_4$ (a) and $CaEu_2(MoO_4)_4$ (b) structures. The insets show the splitting of the main reflection 112 in monoclinic $CaEu_2(WO_4)_4$ and the absence of this splitting in tetragonal $CaEu_2(MoO_4)_4$. Black and green bars mark the positions of the main and satellite reflections, respectively.

Table 1. Selected Crystallographic Data and Refinement Parameters for $CaEu_2(WO_4)_4$ and $CaEu_2(MoO_4)_4$

formula	$CaEu_2(WO_4)_4$	$CaEu_2(MoO_4)_4$
superspace group	$I2/b(\alpha\beta0)00$	$I4_1/a(\alpha\beta0)00(-\beta\alpha0)00$
a, Å	5.23873(1)	5.238672(7)
b, Å	5.26635(1)	–
c, Å	11.46319(9)	11.54843(2)
γ, deg	91.1511(2)	–
$\mathbf{q_1}$	0.56153(6)$\mathbf{a}^*$ + 0.7708(9)$\mathbf{b}^*$	0.55331(8)$\mathbf{a}^*$ + 0.82068(9)$\mathbf{b}^*$
$\mathbf{q_2}$	–	−0.82068(9)$\mathbf{a}^*$ + 0.55331(8)$\mathbf{b}^*$
calcd density, g/cm^3	7.011	5.152
Z	1	1
radiation	synchrotron X-ray, λ = 0.399 96 Å	
2θ range, step, deg	$2 \leq 2\theta \leq 35$; 0.002	$2 \leq 2\theta \leq 40$; 0.002
R_F (all and main refl)	0.050, 0.036	0.061, 0.030
R_F (satellites of order 1)	0.075	0.099
R_P, R_{wP}	0.069, 0.089	0.082, 0.113

Rietveld refinements of the crystal structures were performed with the JANA2006 program.[15] The SXPD profiles were fitted with the pseudo-Voigt profile function with the Gaussian term expressed through the Cagliotti equation, $H_G^2 = U \tan^2 \theta + V \tan \theta + W$, and the Lorentzian part due to microstrain broadening, $H_L = Y \tan \theta$. The larger broadening of the satellite reflections has been accounted

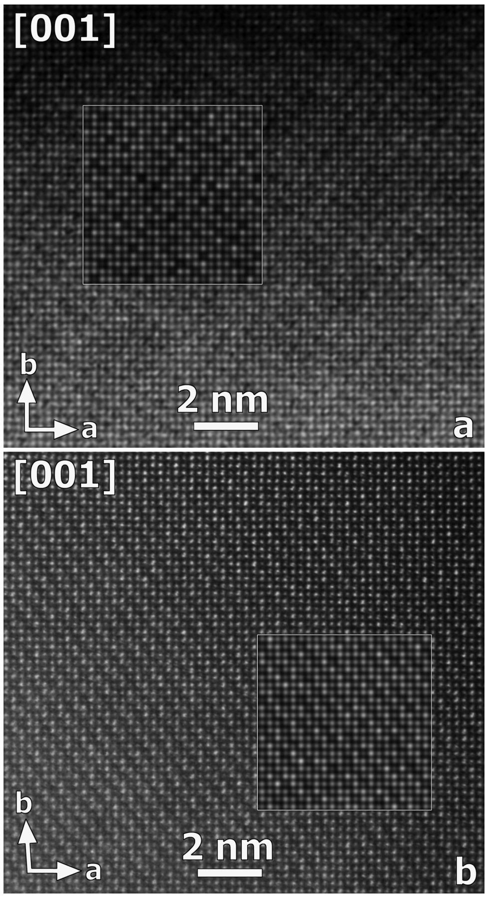

Figure 2. [001] HAADF-STEM images of $CaEu_2(MoO_4)_4$ (a) and $CaEu_2(WO_4)_4$ (b). The calculated images are shown as insets [$CaEu_2(MoO_4)_4$, thickness of 9.1 nm; $CaEu_2(WO_4)_4$, thickness of 5.8 nm)].

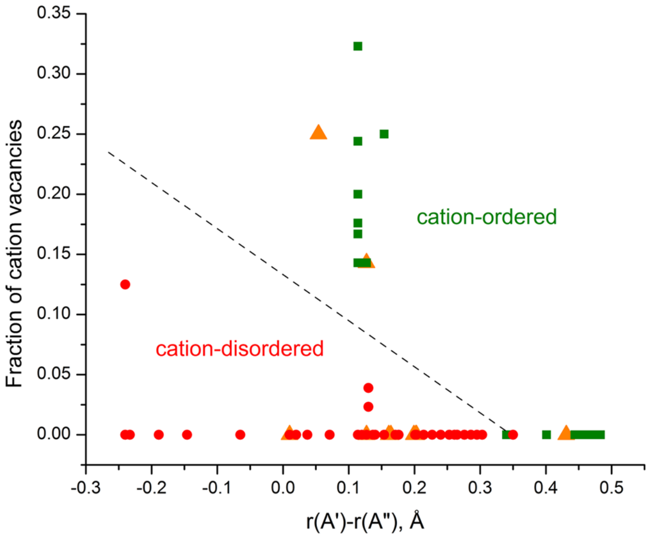

Figure 4. Structure map of the $(A',A'')_{1-x}BO_4$ (B = Mo, W) scheelites demonstrating dependence of the A-site cation ordering on the difference in the ionic radii of the A-cations $r(A') - r(A'')$ and the fraction of the cation vacancies x. The A′ notation stands for the cation with the smaller formal charge, whereas A″ denotes the cations with the larger formal charge. The dashed line separating the ordered and disordered regions is a guide to the eye. Green squares, yellow triangles, and red circles stand for the compounds with complete ordering, partial ordering, and full disorder of the A′- and A″-cations, respectively. The data and corresponding references are given in Table S5 of the Supporting Information.

for with the Stephens formalism adopted for incommensurate phases.[16]

Samples for transmission electron microscopy were made by crushing the powder in an agate mortar and dispersing it in methanol. After treatment in an ultrasonic bath to disperse the crystallites, a few drops of the solution were placed on a copper grid with a holey carbon film. High-resolution high-angle annular dark-field scanning transmission electron microscopy (HAADF-STEM) images were obtained at 300 kV on a FEI Titan 50-80 microscope equipped with a probe aberration corrector. Theoretical HAADF-STEM images were calculated using the QSTEM software.[17]

3. RESULTS

The SXPD patterns of the $CaEu_2(BO_4)_4$ (B = Mo, W) samples were indexed with the unit cell parameters, modulation vectors,

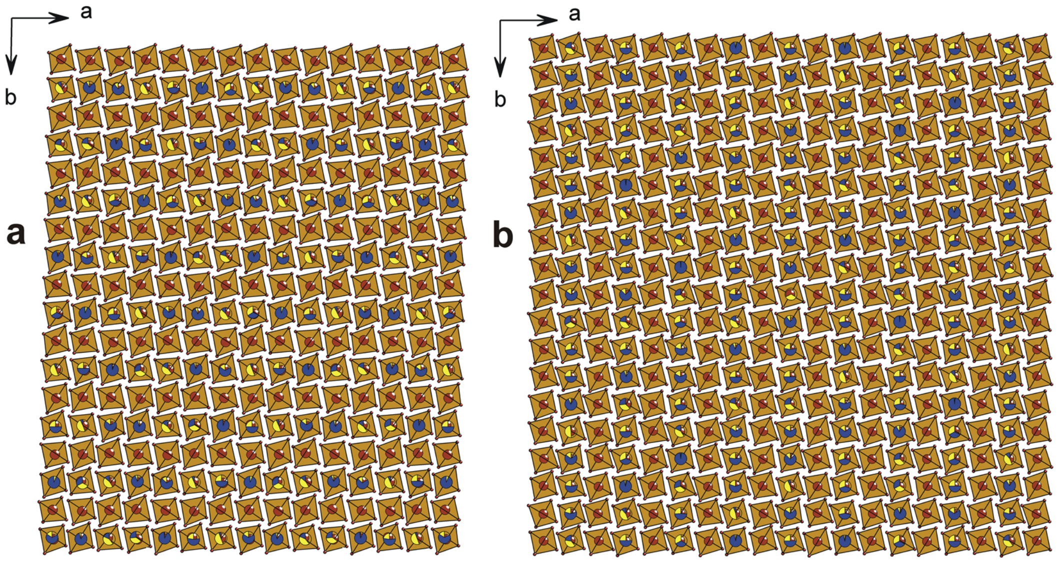

Figure 3. Overview of the crystal structures of $CaEu_2(WO_4)_4$ (7 × 9 supercell) (a) and $CaEu_2(MoO_4)_4$ (9 × 9 supercell) (b). The B = Mo, W atoms are shown as brown spheres. The population of the A-sites is reflected through colored sectors (blue for Eu, yellow for Ca, and transparent for vacancies). The oxygen tetrahedra around the B-cations are drawn.

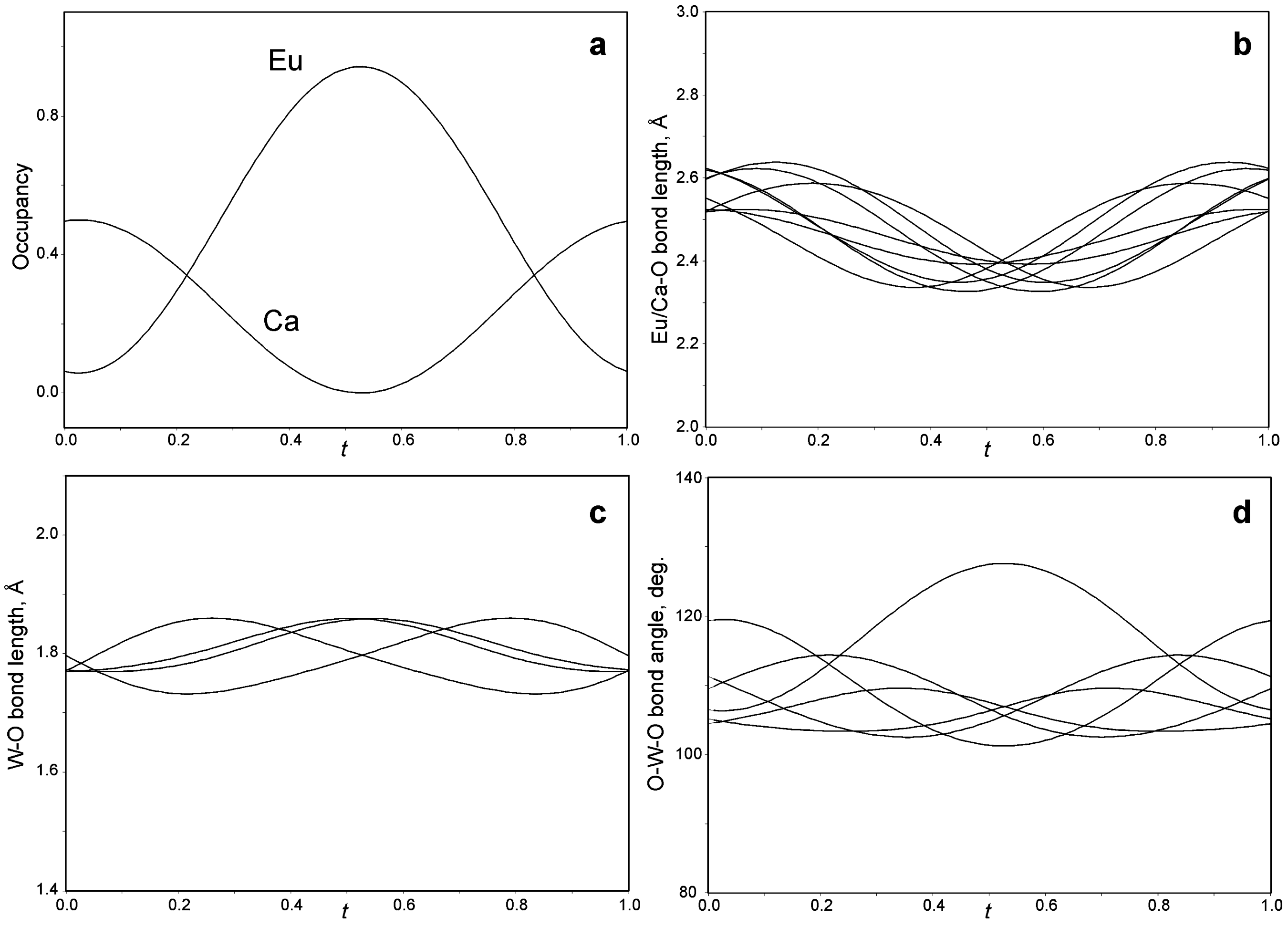

Figure 5. Variation of the Eu/Ca occupancies (a), Eu/Ca−O bond length (b), W−O bond length (c), and O−W−O bond angles (d) in the $CaEu_2(WO_4)_4$ structure represented in the form of *t*-plots.

and superspace symmetry determined earlier with electron diffraction.[13] For $CaEu_2(WO_4)_4$, the expression for the modulation vector was modified in comparison with the literature data in order to exclude an excessive rational component. Previously, a model of the occupancy modulation for monoclinic $CaEu_2(WO_4)_4$ has been constructed using precession electron diffraction (PED) data, but the exact shape of the occupational modulation functions was not determined. Therefore, different models were tested in the Rietveld refinement from the SXPD data:

(i) the occupancy factor of the A-site is modulated harmonically by assuming cation/vacancy ordering only and no Eu/Ca ordering;

(ii) the occupancy factor of the A-site is modulated as a steplike (crenel) function by assuming cation/vacancy ordering only and no Eu/Ca ordering;

(iii) the occupancy factor of the A-site is modulated as a steplike (crenel) function by assuming both cation/vacancy and Eu/Ca ordering, as suggested previously from the PED data [crenel domain of vacancies with $\Delta = {}^{1}/_{4}$ situated at $x_4^0 = {}^{1}/_{2}$ surrounded by two crenel domains of Ca ($x_4^0 = {}^{5}/_{16}$ and $x_4^0 = {}^{11}/_{16}$; $\Delta = {}^{1}/_{8}$ each) and the crenel domain of Eu ($\Delta = {}^{1}/_{2}$ centered at $x_4^0 = 0$)].[13]

Model iii demonstrated much higher reliability factors [R_F(main reflections) = 0.049, R_F(first-order satellites) = 0.104] and was discarded on this basis. The fact that the steplike occupational modulation provides a better fit to the PED data could be due to residual dynamical diffraction effects, which are intrinsic in electron diffraction and in our particular case might result in overestimating the intensities of the satellite reflections. Intensity enhancement of the satellite reflections is visible from a comparison of the (*hk*0)* reciprocal lattice planes in the PED and SXPD experiments (Figure S1 of Supporting Information). Models i and ii revealed identical reliability factors [R_F(main reflections) = 0.036, R_F(first-order satellites) = 0.075], but as soon as intensities of the second-order satellites are calculated, the difference between these models becomes obvious. Model ii with the steplike occupational modulation is in remarkable disagreement with the experiment, providing noticeable intensities of the second-order satellites, which are not visible on the experimental SXPD pattern. Therefore, model i with a harmonic modulation was adopted.

As the same crystallographic position is occupied by three species with different scattering factors (Eu, Ca, and vacancy), their impact in the total modulation of the scattering density at this position cannot be resolved unambiguously. Taking the occupancy modulation function as $p^{\lambda} = p_0^{\lambda} + p_1^{\lambda}\cos(2\pi x_4)$, $x_4 = \mathbf{q}\mathbf{r}^{\lambda} + t$ ($\mathbf{r}^{\lambda}$ is the position of the atom λ in the basic structure, t is an internal phase), the p_0 values for the Eu and Ca atoms can be determined directly from the diffraction experiment, whereas the p_1 parameters can change in a certain interval without affecting the scattering density distribution and reliability factors. The detailed procedure of the estimation of the p_0^{λ} and p_1^{λ} parameters

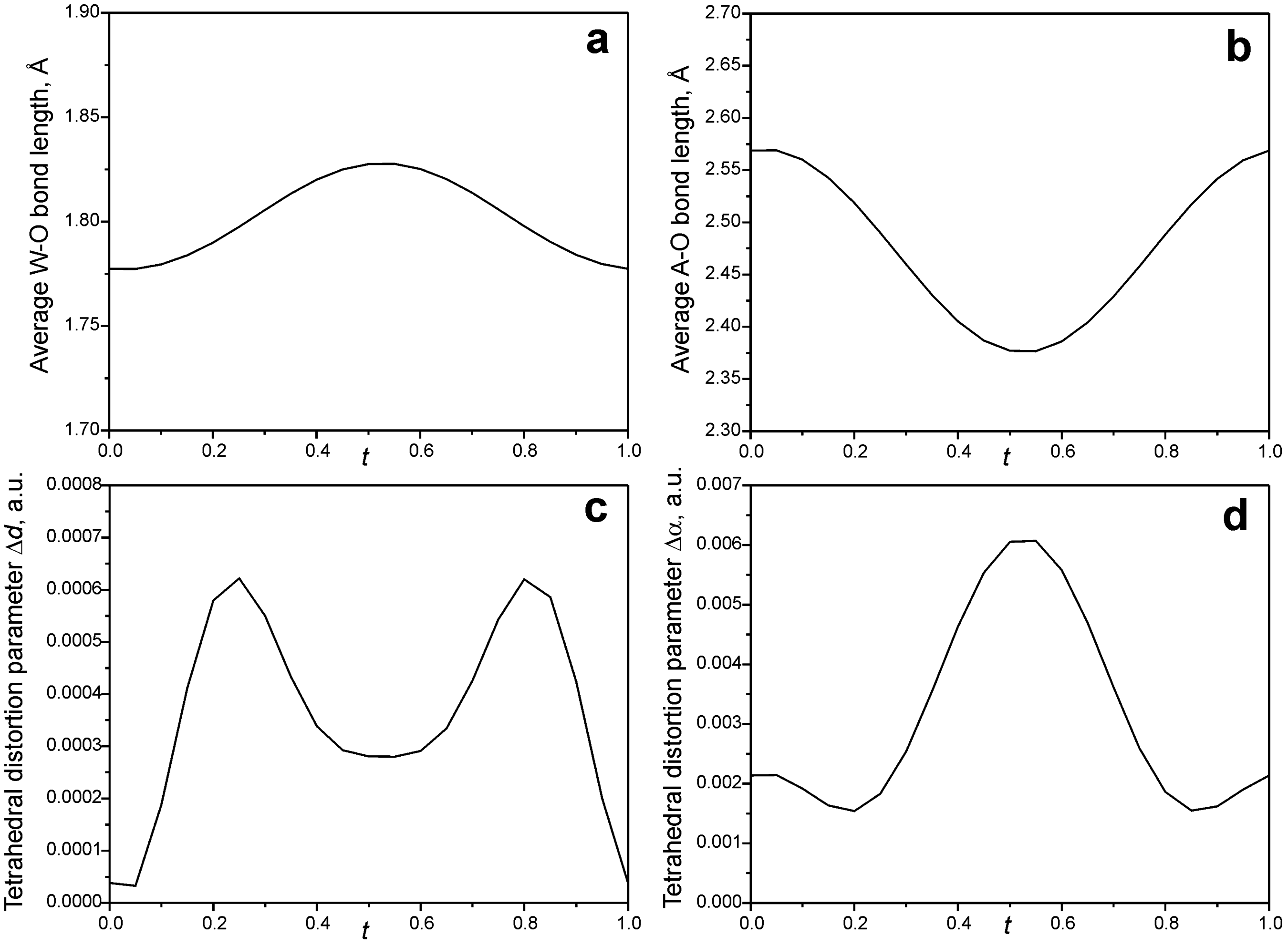

Figure 6. Variation of the average W−O bond length (a), average A−O bond length (b), and tetrahedral distortion parameters Δ*d* (c) and Δ*α* (d) in the $CaEu_2(WO_4)_4$ structure represented in the form of *t*-plots.

is given in the Supporting Information and can be summarized as following:

(1) the scattering density modulation has been refined as $\rho = [p_0 + p_1 \cos(2\pi x_4)]Z^{Eu}$;

(2) the p_0^{λ} parameters for the Ca and Eu positions were calculated from the refined occupancy modulation wave;

(3) the physically meaningful interval for the p_1^{λ} parameters was estimated by taking into account that the total occupancy of the A position cannot exceed 1 and the occupancy modulation functions for both Eu and Ca cannot acquire negative values.

The experimentally determined modulation of the scattering density at the A position agrees only with an antiphase occupancy modulation of the Eu and Ca atoms. Following the analysis given in the Supporting Information, the values of $p_0^{Eu} = 0.5$, $p_0^{Ca} = 0.25$, $p_1^{Eu} = 0.4433$, and $p_1^{Ca} = -0.25$ were accepted.

Because no satellites with an order higher than 1 were observed on the SXPD pattern of $CaEu_2(WO_4)_4$, the displacive modulation was fitted with a first-order harmonic. Parameters of the modulation functions that did not exceed their standard deviations were fixed to 0 in the refinement. Identical atomic coordinates and atomic displacement parameters (ADPs) were refined for the Eu and Ca atoms. The oxygen atoms were refined with a common ADP.

A similar refinement strategy has been applied to the $CaEu_2(MoO_4)_4$ structure. In contrast to monoclinic $CaEu_2(WO_4)_4$, its Mo-based counterpart adopts a tetragonal symmetry and requires two symmetrically related modulation vectors to index the diffraction pattern. The tetragonal symmetry of $CaEu_2(MoO_4)_4$ is obvious from the absence of the monoclinic splitting of the 112 main reflection (Figure 1). Such splitting is very prominent on the SXPD pattern of monoclinic $CaEu_2(WO_4)_4$. The clear presence of the *hklmn* satellite reflections with $|m| = 1$ and $|n| = 1$ was evident from the electron diffraction patterns of $CaEu_2(MoO_4)_4$, justifying the selection of the (3+2)D superspace model.[13] However, such satellites are almost invisible on the SXPD pattern: only two $101\bar{1}1$ and $200\bar{1}1$ satellites with a relative intensity ≤0.05% were reliably detected. Thus, only the modulation waves corresponding to $|m| = 1$, $|n| = 0$ and $|m| = 0$, $|n| = 1$ were used in the refinement. The parameters of the occupancy modulation waves of the Eu and Ca atoms were assigned similarly as in the $CaEu_2(WO_4)_4$ structure.

The crystallographic information on the $CaEu_2(BO_4)_4$ (B = Mo, W) compounds is provided in Table 1, the atomic parameters and coefficients of the modulation functions are listed in Tables S1 and S2 of the Supporting Information. The main interatomic distances are given in Tables S3 and S4 of the Supporting Information. The experimental, calculated, and difference SXPD profiles after the Rietveld refinement are shown in Figure 1.

The refined structures have been confirmed using high-resolution HAADF-STEM images (Figure 2). The [001] HAADF-STEM images provide a clear image of the occupational modulation wave, even in spite of the fact that the Ca/Eu and B positions are projected onto each other. These atomic columns form a prominent rectangular pattern of bright dots on both images. The occupational modulation waves in CaEu$_2$(MoO$_4$)$_4$ are visible on the HAADF-STEM image (Figure 2a) as a cross-cutting pattern of alternating stripes of brighter and darker dots, in agreement with the tetragonal symmetry of this compound. In the image of monoclinic CaEu$_2$(WO$_4$)$_4$ only one system of parallel stripes is visible (Figure 2b). The simulated HAADF-STEM images calculated using 20 × 20 supercells are in good agreement with the experimental ones (see insets in Figure 2a,b).

4. DISCUSSION

Overview images of the CaEu$_2$(BO$_4$)$_4$ (B = Mo, W) structures are shown in Figure 3. As in many other scheelite-type molybdates and tungstates, the primary modulation in these compounds originates from the ordering at the A sublattice. The A-site cation ordering can be realized in the scheelites with or without A-site cation vacancies. In the stoichiometric A′A″(BO$_4$)$_2$ (B = Mo, W) scheelites with a complete occupation of the A-positions there is a clear threshold between the structures with ordered and disordered arrangement of the A-cations: the ordering occurs for the A′- and A″-cations that differ in the ionic radii by more than $\Delta r \sim 0.35$ Å (Figure 4). However, not only the absolute value of the r(A′) − r(A″) difference is important but also its sign: the ordering occurs only if the A′-cation with the smaller formal charge is larger than the A″-cation with the higher formal charge. The requirement for the size difference is significantly relaxed if cation vacancies are present in the A position and if the ordering of the A′- and A″-cations is coupled with the cation/vacancy ordering. Then the A′/A″-ordering is observed at Δr as small as ∼0.1 Å. These cation-deficient scheelites form a separate cluster on the structure map built in the coordinates Δr−fraction of cation vacancies (Figure 4). The CaEu$_2$(BO$_4$)$_4$ (=CaEu$_2$□(BO$_4$)$_4$, B = Mo, W; □ = A-site vacancy) structures (Δr = 0.054 Å, 25% of vacancies) also belong to this cluster. Indeed, the antiphase Ca and Eu occupancy modulations in both compounds reflect that the partial Ca/Eu ordering takes place and is coupled to the ordering between the cations and vacancies. The charge difference Δq between the A′- and A″-cations should also influence their order, but the overwhelming majority of the (A′,A″)$_{1-x}$BO$_4$ scheelites feature $\Delta q = 2$ which does not allow us to track the dependence of the ordering on the charge difference. One can think that the tendency to optimize the bond valence balance for the A-cations and oxygen atoms serves as the main driving force for the compositional modulation. Although the incomplete cation ordering in the CaEu$_2$(BO$_4$)$_4$ (B = Mo, W) structures prevents precise analysis of the bond valences, some common trends in variation of the interatomic distances and angles can be picked up.

The main structural parameters in CaEu$_2$(WO$_4$)$_4$ are presented in Figure 5 in the form of t-plots providing a comprehensive overview of the variation of the parameters in different unit cells of the basic structure.[18] The occupancy modulation waves for the Eu and Ca atoms demonstrate an antiphase relation, peaked at $t \approx {}^1/_2$ and $t \approx 0$, respectively (Figure 5a). The Eu/Ca−O interatomic distances in the AO$_8$ coordination polyhedra vary in the range of ∼0.3 Å (Figure 5b and Table S2 of the Supporting Information). It should be noted that all eight A−O distances change nearly concomitantly, pointing toward a breathing distortion of the AO$_8$ polyhedron rather than to off-center shifts of the A-cation. The W−O interatomic distances in the WO$_4$ tetrahedra are more rigid, demonstrating a maximum spread of ∼0.13 Å (Figure 5c and Table S2, Supporting Information), which is insufficient to compensate for the variation of the A−O separations. This compensation could be achieved through rotations and displacements of the WO$_4$ units as a whole or through changing the O−W−O bond angles. In order to verify the former possibility, we have performed the refinement of the CaEu$_2$(WO$_4$)$_4$ structure in a rigid body approximation, where the displacements and rotations of the whole WO$_4$ tetrahedron were harmonically modulated while at the same time constant interatomic distances and bond angles as in the average structure were maintained. The refinement revealed less favorable reliability factors [R_F(main reflections) = 0.037, R$_F$(first-order satellites) = 0.078] and larger ADPs for the oxygen atoms [U_{iso} = 0.023(1)Å^2]. Although the refinements with soft and rigid WO$_4$ units do not differ drastically, we tend to adopt the results of the unrestrained refinement. This conclusion is corroborated by the analysis of the cation-vacancy ordered Eu$_2$(WO$_4$)$_3$ sheelite-type structure.[19] In this structure, the spread of the W−O interatomic distances (0.08−0.09 Å) is

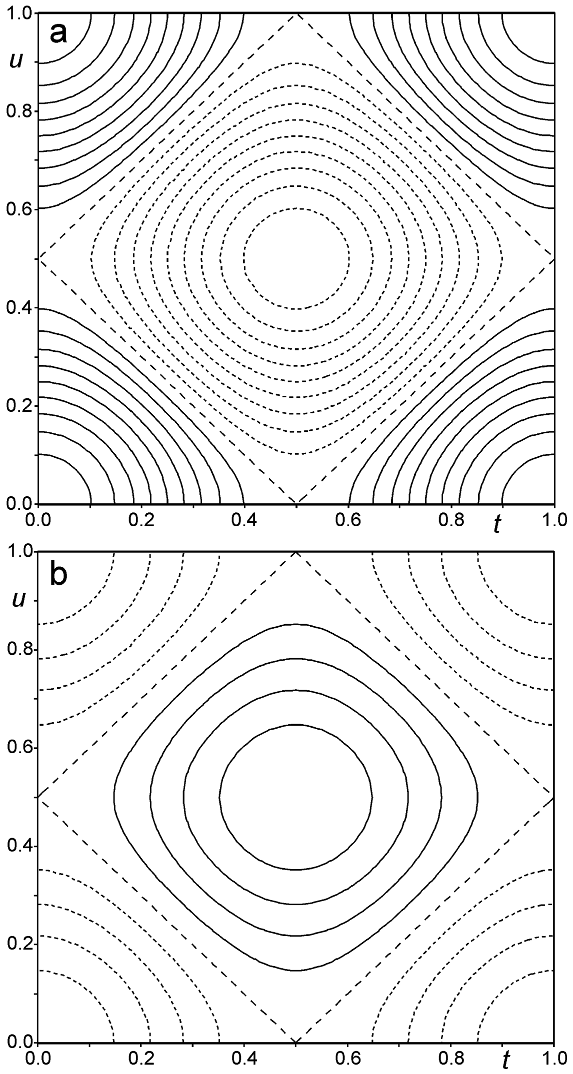

Figure 7. Variation of the Eu/Ca occupancies in the CaEu$_2$(MoO$_4$)$_4$ structure represented in the form of t−u-plots. The Eu occupancy (a) varies between 0 and 1 (solid and dotted contours mark the occupancy factor $>{}^1/_2$ and $<{}^1/_2$, respectively, and dashed contour marks the occupancy factor of ${}^1/_2$), the Ca occupancy (b) varies between 0 and ${}^1/_2$ (solid and dotted contours mark the occupancy factor $>{}^1/_4$ and $<{}^1/_4$, respectively, and dashed contour marks the occupancy factor of ${}^1/_4$).

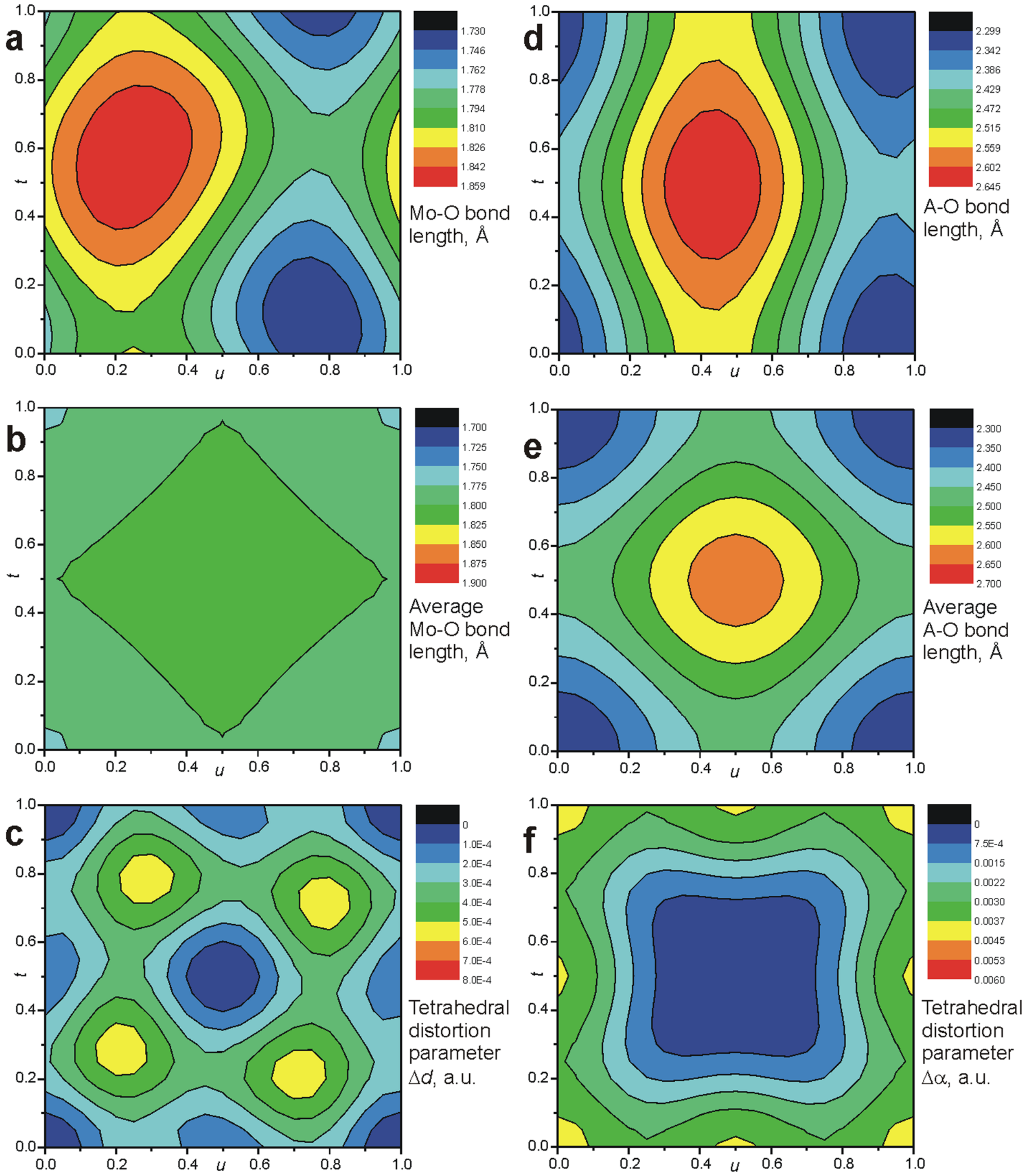

Figure 8. Variation of the interatomic distances in the $CaEu_2(MoO_4)_4$ structure represented as color-coded t–u-plots: Mo–O bond length (a), average Mo–O bond length (b), MoO_4 tetrahedral distortion parameter Δd (c), A–O bond length (d), average A–O bond length (e), and MoO_4 tetrahedral distortion parameter $\Delta\alpha$ (f).

somewhat smaller, but comparable to that in $CaEu_2(WO_4)_4$. The O–W–O bond angles in $Eu_2(WO_4)_3$ deviate significantly from the perfect tetrahedral angle of 109.5°, varying in the range of 103°–121°. This is comparable to the variation of the tetrahedral angles in $CaEu_2(WO_4)_4$ (Figure 5d).

The t-plots of the integral structural parameters for $CaEu_2(WO_4)_4$ are shown in Figure 6. The average Eu/Ca–O and W–O distances demonstrate an antiphase variation (Figure 6a,b). The increasing occupancy of the A-site with the Eu^{3+} cations causes a significant contraction of the average Eu/Ca–O distance and a concomitant expansion of the W–O bond lengths. This tendency agrees with the smaller ionic radius of the Eu^{3+} cations (r = 1.066 Å, CN = 8) compared to that of Ca^{2+} (r = 1.12 Å, CN = 8).[20] The elongation of the average W–O bond length is nearly 4 times smaller than the contraction of the Eu/Ca–O distance and cannot fully compensate it. We analyzed the distortion of the WO_4 unit with the tetrahedral distortion parameters Δd and $\Delta\alpha$, characterizing the deviations of the W–O interatomic distances from the average value and the deviations of the O−W−O bond angles from the perfect tetrahedral angle. The parameters are defined as

$$\Delta d = 1/4 \sum_{n=1-4} [(d_n - d)/d]^2$$

$$\Delta \alpha = 1/6 \sum_{n=1-6} [(\alpha_n - \alpha)/\alpha]^2$$

where d_n is the individual W−O bond length, d is the average W−O bond length, α_n is the individual O−W−O bond angle, and α is the perfect tetrahedral angle (Figure 6c,d). As intuitively expected from a comparison with the $Eu_2(WO_4)_3$ structure, the maximum angular distortion of the WO_4 tetrahedra coincides with the maximum occupation of the A positions by the Eu atoms. At the same time, the maximum spread of the W−O distances occurs in the unit cells with the minimal angular distortion. This demonstrates that the behavior of the WO_4 units is far from that expected in the rigid body approximation. The structure adopts the variable size and charge of the cations at the A-position through the deformation of the WO_4 tetrahedra, which occurs as an antiphase alternation of two distortion modes with either stretching of the W−O bonds or bending of the O−W−O bond angles.

Similar trends are also observed in the $CaEu_2(MoO_4)_4$ structure. The Ca and Eu occupancy factors are modulated in an antiphase manner (Figure 7a, b). The A−O distances vary significantly, being smallest at the unit cells with the highest Eu occupancy (Figure 8d,e) and largest when the A-site is populated by Ca and vacancies. The MoO_4 tetrahedra do not behave as rigid units: the variation of the Mo−O interatomic distances is comparable to that in the WO_4 tetrahedra (Figure 8a and Table S4 of Supporting Information), although the variation of the average Mo−O distance is relatively small (Figure 8b), particularly in comparison with the variation of the average A−O distance (Figure 8e). The tetrahedral distortion parameters Δd and $\Delta\alpha$ demonstrate trends similar to those in the $CaEu_2(WO_4)_4$ structure. The smallest stretching distortion of the Mo−O bonds (minimal values of Δd) occurs in the unit cells with the highest Eu or Ca content (Figure 8c), and the largest bending distortion of the O−Mo−O angles (largest $\Delta\alpha$) occurs in the unit cells with the highest Eu content. Similar behavior of the MoO_4 units can also be observed in other modulated scheelites. The minimum and maximum Mo−O interatomic distances and O−Mo−O angles in the A-site ordered scheelites $KNd(MoO_4)_2$, $KSm(MoO_4)_2$, $Na_{2/7}Gd_{4/7}MoO_4$, and $Eu_2(MoO_4)_3$ indicate that the "stretching" and "bending" distortion modes are significant in these structures as well.[9,10,12,21]

In conclusion, the refinements of the $CaEu_2(WO_4)_4$ and $CaEu_2(MoO_4)_4$ structures reveal that the MoO_4^{2-} and WO_4^{2-} tetrahedra in scheelites demonstrate a flexible geometry. Both the metal−oxygen distances and bond angles vary significantly with changing the population of the A-site by cations with different charge/size and/or cation vacancies. It should be noted that the flexibility of the tetrahedral units in the cation-ordered scheelites differs drastically from the quite rigid behavior of these units in scheelites under external pressure.[22−24] The fluctuating geometry of the tetrahedral units can be a means for adjusting the bond valence sum at the oxygen atoms in cation-ordered scheelites and, thus, serves as a medium for transferring interactions between ordered, differently populated A-sites. One may speculate that ab initio calculations of the energy cost for different deformation modes of the MoO_4^{2-} and WO_4^{2-} tetrahedra depending on the local crystal environment would be the key for rationalizing the ordering patterns in scheelites.

■ ASSOCIATED CONTENT

Ⓢ Supporting Information

The (*hk*0)* reciprocal lattice planes for $CaEu_2(WO_4)_4$ taken with PED and SXPD; analysis of the occupancy modulation in the $CaEu_2(WO_4)_4$ structure; atomic coordinates, amplitudes of Fourier components of the modulation functions, isotropic atomic displacement parameters and main interatomic distances for $CaEu_2(WO_4)_4$ and $CaEu_2(MoO_4)_4$; overview of the A-site ordered and A-site disordered scheelite-type structures; CIF files for $CaEu_2(WO_4)_4$ and $CaEu_2(MoO_4)_4$. This material is available free of charge via the Internet at http://pubs.acs.org.

■ AUTHOR INFORMATION

Corresponding Author

*E-mail: artem.abakumov@uantwerpen.be. Tel: +32(3) 2653259.

Notes

The authors declare no competing financial interest.

■ ACKNOWLEDGMENTS

This research was supported by FWO (project G039211N), Flanders Research Foundation. V.M. is grateful for financial support of the Russian Foundation for Basic Research (Grants 12-03-00124 and 14-03-01100). We are grateful to the ESRF for granting the beamtime. Experimental support of Andy Fitch at the ID31 beamline of ESRF is kindly acknowledged.

■ REFERENCES

(1) Su, Y.; Li, P.; Li, G. *Chem. Mater.* **2008**, *20*, 6060−6067.

(2) Wang, Z.; Zhang, Y.; Xiong, L.; Li, X.; Guo, J.; Gong, M. *Curr. Appl. Phys.* **2012**, *12*, 1084−1087.

(3) Liu, Y.; Lu, Z.-G.; Gu, Y.-Y.; Li, W. *J. Lumin.* **2012**, *132*, 1220−1225.

(4) Qin, L.; Huang, Y.; Tsuboi, T.; Seo, H. J. *Mater. Res. Bull.* **2012**, *47*, 4498−4502.

(5) Chen, Y. J.; Lin, Y. F.; Guo, W. J.; Gong, X. H.; Huang, J. H.; Luo, Z. D.; Huang, Y. D. *Laser Phys. Lett.* **2012**, *9*, 141−144.

(6) Yu, Y.; Zhang, L.; Huang, Y.; Lin, Z.; Wang, G. *Laser Phys.* **2013**, *23*, 105807.

(7) Arakcheeva, A.; Logvinovich, D.; Chapuis, G.; Morozov, V.; Eliseeva, S. V.; Bünzli, J.-C. G.; Pattison, P. *Chem. Sci.* **2012**, *3*, 384.

(8) Zhao, W.; Zhou, W.-W.; Wei, B.; Wang, G. F. *Phys. Status Solidi Sect. B* **2013**, *210*, 367−372.

(9) Morozov, V. A.; Arakcheeva, A. V.; Chapuis, G.; Guiblin, N.; Rossell, M. D.; Van Tendeloo, G. *Chem. Mater.* **2006**, *18*, 4075−4082.

(10) Arakcheeva, A.; Pattison, P.; Chapuis, G.; Rossell, M.; Filaretov, A.; Morozov, V.; Van Tendeloo, G. *Acta Cryst. B* **2008**, *64*, 160−171.

(11) Morozov, V. A.; Mironov, A. V.; Lazoryak, B. I.; Khaikina, E. G.; Basovich, O. M.; Rossell, M. D.; Van Tendeloo, G. *J. Solid State Chem.* **2006**, *179*, 1183−1191.

(12) Morozov, V.; Arakcheeva, A.; Redkin, B.; Sinitsin, V.; Khasanov, S.; M. Raskina, M.; Lebedev, O.; Van Tendeloo, G. *Inorg. Chem.* **2012**, *51*, 5313−5324.

(13) Morozov, V. A.; Bertha, A.; Meert, K. W.; Van Rompaey, S.; Batuk, D.; Martinez, G. T.; Van Aert, S.; Smet, P. F.; Raskina, M. V.; Poelman, D.; Abakumov, A. M.; Hadermann, J. *Chem. Mater.* **2013**, *25*, 4387−4395.

(14) Meert, K. W.; Morozov, V. A.; Abakumov, A. M.; Hadermann, J.; Poelman, D.; Smet, P. F. *Optic Express* **2014**, *22*, A961−A972.

(15) Petricek, V.; Dusek, M.; Palatinus, L. *Jana2006. The Crystallographic Computing System*; Institute of Physics: Praha, Czech Republic, 2006.

(16) Leineweber, A.; Petricek, V. J. *Appl. Cryst.* **2007**, *40*, 1027−1034.

(17) Koch, C. Determination of Core Structure Periodicity and Point Defect Density along Dislocations. Ph.D. dissertation; Arizona State University, Phoenix, AZ, 2002.

(18) van Smaalen, S. *Incommensurate Crystallography*; Oxford University Press: New York, 2007.

(19) Templeton, D. H.; Zalkin, A. *Acta Crystallogr.* **1963**, *16*, 762−766.

(20) Shannon, R. D. *Acta Crystallogr.* **1976**, *A32*, 751−767.

(21) Boulahya, K.; Parras, M.; Gonzalez Calbet, J. M. *Eur. J. Inorg. Chem.* **2005**, 967−970.

(22) Hazen, R. M.; Finger, L. W.; Mariathasan, J. W. E. *J. Phys. Chem. Solids* **1985**, *46*, 253−263.

(23) Errandonea, D.; Kumar, R. S.; Ma, X.; Tu, C. *J. Solid State Chem.* **2008**, *181*, 355−364.

(24) Achary, S. N.; Patwe, S. J.; Mathews, M. D.; Tyagi, A. K. *J. Phys. Chem. Solids* **2006**, *67*, 774−781.